AMERICAN SOCIETY FOR MICROBIOLOGY | Journal of Virology®

VIRUS-CELL INTERACTIONS

Cellular RNA Helicase DHX9 Interacts with the Essential Epstein-Barr Virus (EBV) Protein SM and Restricts EBV Lytic Replication

Wenmin Fu,[a] Dinesh Verma,[a] Ashlee Burton,[a] Sankar Swaminathan[a,b]

[a]Division of Infectious Diseases, Department of Medicine, University of Utah School of Medicine, Salt Lake City, Utah, USA
[b]George E. Wahlen Department of Veterans Affairs Medical Center, Salt Lake City, Utah, USA

ABSTRACT Epstein-Barr virus (EBV) SM protein is an RNA-binding protein that has multiple posttranscriptional gene regulatory functions essential for EBV lytic replication. In this study, we identified an interaction between SM and DHX9, a DExH-box helicase family member, by mass spectrometry and coimmunoprecipitation. DHX9 participates in many cellular pathways involving RNA, including transcription, processing, transport, and translation. DHX9 enhances virus production or infectivity of a wide variety of DNA and RNA viruses. Surprisingly, an increase in EBV late gene expression and virion production occurred upon knockdown of DHX9. To further characterize the SM-DHX9 interaction, we performed immunofluorescence microscopy of EBV-infected cells and found that DHX9 partially colocalized with SM in nuclear foci during EBV lytic replication. However, the positive effect of DHX9 depletion on EBV lytic gene expression was not confined to SM-dependent genes, indicating that the antiviral effect of DHX9 was not mediated through its effects on SM. DHX9 enhanced activation of innate antiviral pathways comprised of several interferon-stimulated genes that are active against EBV. SM inhibited the transcription-activating function of DHX9, which acts through cAMP response elements (CREs), suggesting that SM may also act to counteract DHX9's antiviral functions during lytic replication.

IMPORTANCE This study identifies an interaction between Epstein-Barr virus (EBV) SM protein and cellular helicase DHX9, exploring the roles that this interaction plays in viral infection and host defenses. Whereas most previous studies established DHX9 as a proviral factor, we demonstrate that DHX9 may act as an inhibitor of EBV virion production. DHX9 enhanced innate antiviral pathways active against EBV and was needed for maximal expression of several interferon-induced genes. We show that SM binds to and colocalizes DHX9 and may counteract the antiviral function of DHX9. These data indicate that DHX9 possesses antiviral activity and that SM may suppress the antiviral functions of DHX9 through this association. Our study presents a novel host-pathogen interaction between EBV and the host cell.

KEYWORDS Epstein-Barr virus, RNA processing, helicase, innate immune response, protein-protein interactions, transcriptional activation, virus-host interactions

Epstein-Barr virus (EBV), a human gammaherpesvirus, has been implicated as a major cause of infectious mononucleosis, lymphoproliferative disorders, and lymphoid and epithelial malignancies (1). EBV establishes a lifelong latent persistent infection in over 90% of human adults. Memory B lymphocytes are the site of latent infection, from which EBV intermittently reactivates, entering a lytic phase of replication that culminates in production of infectious virions that are shed in saliva. Several lines of evidence implicate lytic replication in EBV pathogenesis. In addition to being required for horizontal transmission, production of infectious virions may be important for main-

Citation Fu W, Verma D, Burton A, Swaminathan S. 2019. Cellular RNA helicase DHX9 interacts with the essential Epstein-Barr virus (EBV) protein SM and restricts EBV lytic replication. J Virol 93:e01244-18. https://doi.org/10.1128/JVI.01244-18.

Editor Richard M. Longnecker, Northwestern University

Address correspondence to Sankar Swaminathan, sankar.swaminathan@hsc.utah.edu.

Received 13 August 2018
Accepted 28 November 2018
Accepted manuscript posted online 12 December 2018
Published 5 February 2019

taining the latent EBV reservoir (2). In addition, lytic replicative proteins are increasingly recognized as playing a role in tumorigenesis (3, 4). Therefore, understanding the molecular mechanisms that regulate EBV lytic replication and gene expression is important for investigating EBV pathogenesis.

The EBV early nuclear protein SM (EB2, BMLF1, Mta) has multiple posttranscriptional gene regulatory functions that are essential for lytic EBV replication (5–9). SM is an RNA-binding protein that shuttles between the nucleus and the cytoplasm and posttranscriptionally increases mRNA accumulation of its target mRNAs (6, 7, 10). SM preferentially enhances expression of approximately 15 late EBV mRNAs, many of which are essential for viral encapsidation and infectivity (11). SM facilitates EBV gene expression by stabilizing mRNA and promoting nuclear mRNA export (6, 12–14). SM interacts with cellular export proteins, thus acting as a bridge between intronless viral mRNAs and the cellular export machinery, preferentially facilitating expression of viral lytic mRNAs over cellular intron-containing mRNAs (15, 16). SM has also been shown to affect mRNA splicing by recruiting cellular splicing factor SRp20 (9) and to enhance translation of specific EBV mRNAs (17). Due to the multiple crucial roles that SM plays in EBV lytic replication, we set out to determine which host cell factors SM utilizes in these functions. In previous studies, we developed an affinity purification and mass spectrometry protocol to isolate SM complexes in order to identify cellular SM-interacting proteins (9). Using this method, RNA helicase A (RHA, DHX9) was identified as a major SM-binding protein.

DHX9, a DExH box helicase family member, participates in nearly every cellular pathway involving RNA, including transcription, processing, transport, and translation (18). The general functional domains of DExH box helicases consist of a core helicase domain, two double-stranded RNA (dsRNA) binding domains (RBDs), a minimal transactivation domain that interacts with RNA polymerase (pol) II, an oligonucleotide binding fold (OBD), nuclear export and nuclear localization signals (NES and NLS, respectively), and an RGG box (19). DHX9 is able to unwind both RNA and DNA duplexes and RNA-DNA hybrids but acts more efficiently on RNA duplexes (20). DHX9 interacts with an extremely large number of cellular partners, most of which can be grouped as being involved in transcription, DNA replication, RNA processing, miRNA biology, and viral replication or viral RNA transport (21–26). DHX9 also directly binds several RNA motifs, modulating transcription, RNA transport, or translation (27–30). DHX9 facilitates several aspects of virus production and infectivity of a broad range of viruses. DHX9 interacts directly with the HIV TAR RNA element to stimulate transcription (21, 24). It also binds the constitutive transport element (CTE) of type D retroviruses and facilitates nuclear export by cooperating with cellular shuttling proteins Tap and HAP95 (26, 29, 31, 32). Similarly, it cooperates with HIV Rev and Sam68 to enable HIV RNA export via the Rev-responsive element (RRE) (23, 27, 28, 33). The helicase function of DHX9 is also required for efficient translation of viral and cellular mRNA with a 5′ posttranscriptional element (PCE) (34). DHX9 binds to mRNAs of human cytomegalovirus (35), adenovirus (36), and hepatitis E virus (37), although the functional implications of these interactions remain to be fully characterized. DHX9 enhances virus production or infectivity of a wide variety of RNA and DNA viruses, such as influenza virus and swine fever virus (25, 38). Although DHX9 has primarily been described as a proviral factor, it may have antiviral properties as well. Knockdown (KD) of several cellular helicases, including DHX9, enhances maximal myxoma virus (MYXV) production (39). Some antiviral properties of DHX9 have been ascribed to its role in the antiviral innate immune response, where it may act as a sensor for dsRNA, enhancing the interferon (IFN) response to viral infection (30, 40). Because of its complex interactions with RNA, its importance in viral biology, and our finding that DHX9 interacts with SM, an essential EBV RNA-binding protein, we investigated the function of DHX9 in SM-mediated EBV gene expression and EBV virion production.

RESULTS

SM interacts directly with DHX9. We previously developed and validated a method to identify SM-interacting cellular proteins by affinity purification of EBV SM

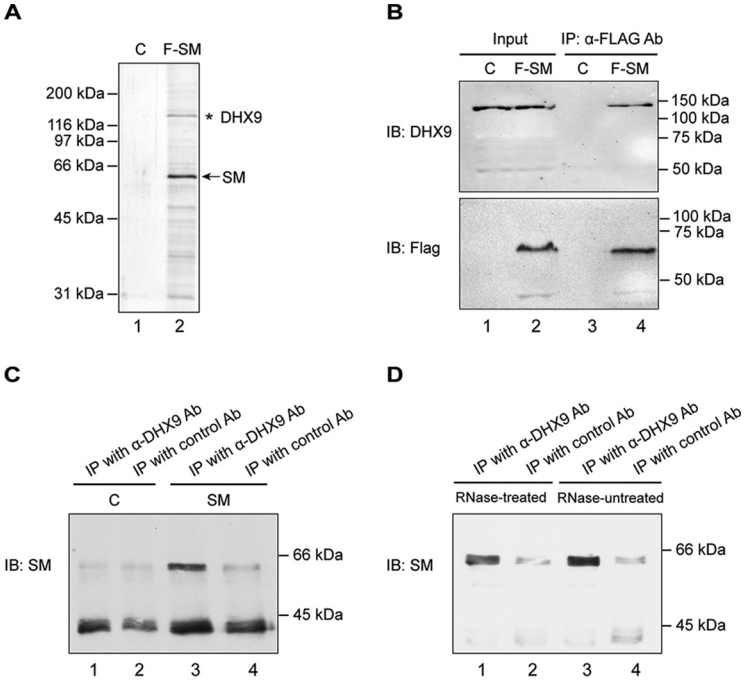

FIG 1 DHX9 interacts with EBV SM protein in an RNase-independent manner. (A) Immunoprecipitation of SM-interacting proteins for mass spectrometry analysis (9). FLAG epitope-tagged SM (F-SM) or empty vector (C) was transfected into 293T cells, and SM was isolated by affinity purification with M2 anti-FLAG antibody-conjugated beads, followed by elution with FLAG peptide. Eluates of lysates from vector-transfected and SM-transfected cells were analyzed by SDS-PAGE and silver staining. The major SM band is shown with an arrow in lane 2. DHX9, which was confirmed by excision of the gel band and MS analysis, is shown with an asterisk. (B) Coimmunoprecipitation of SM and DHX9. 293T cells were transfected with epitope-tagged SM (F-SM) or empty vector (C), and lysates were harvested at 48 h posttransfection. The input protein samples (Input, 0.5% lysate) and samples that were immunoprecipitated with anti-FLAG antibodies (IP, 5% lysate) (lanes 3 and 4) were separated by SDS-PAGE and analyzed by immunoblotting with anti-DHX9 and anti-FLAG antibodies, respectively. (C) Reciprocal immunoprecipitation of SM by DHX9 antibody. 293T cells were transfected with untagged SM or empty vector (C) and then harvested at 48 h posttransfection. The protein samples were immunoprecipitated with anti-DHX9 antibody or control antibody as indicated and analyzed by Western blotting with anti-SM antibody. (D) RNase resistance of DHX9-SM interaction. 293T cells were transfected with untagged SM plasmid, and lysates were harvested at 48 h posttransfection. The protein samples were treated or mock treated with RNase, immunoprecipitated with anti-DHX9 antibody or control antibody, and immunoblotted for SM as in panel C. Molecular weight markers are shown in kilodaltons.

protein complexes (9). 293T cells were transfected with a FLAG epitope-tagged SM expression vector, and protein complexes containing SM were isolated by affinity purification with anti-FLAG antibody-conjugated beads. The eluates from purification were analyzed by silver staining of polyacrylamide gels and revealed multiple SM-associated proteins (Fig. 1A) (data have also been previously shown in reference 9). Mass spectrometry analysis of the immunoprecipitates identified DHX9 as a major SM-interacting protein which was visible on silver-stained gels (Fig. 1A). To validate the mass spectrometry results and confirm the interaction between SM and DHX9, we performed a coimmunoprecipitation assay. 293T cells were transfected with FLAG epitope-tagged SM, and lysates were harvested at 48 h posttransfection. The input protein samples and samples that were immunoprecipitated with anti-FLAG antibody were analyzed by immunoblotting with anti-FLAG or anti-DHX9 antibody. As expected, FLAG-SM was detected by anti-FLAG antibody as a protein of approximately 60 kDa in cells transfected with FLAG-SM but not with empty vector. DHX9 was detected as a protein of 140 kDa that coimmunoprecipitated with SM (Fig. 1B, lanes 2 and 4). In contrast, no DHX9 was coimmunoprecipitated from control cells transfected with empty vector (Fig. 1B, lanes 1 and 3). In order to confirm the specificity of the immunoprecipitation assay, we performed a reciprocal experiment with an untagged

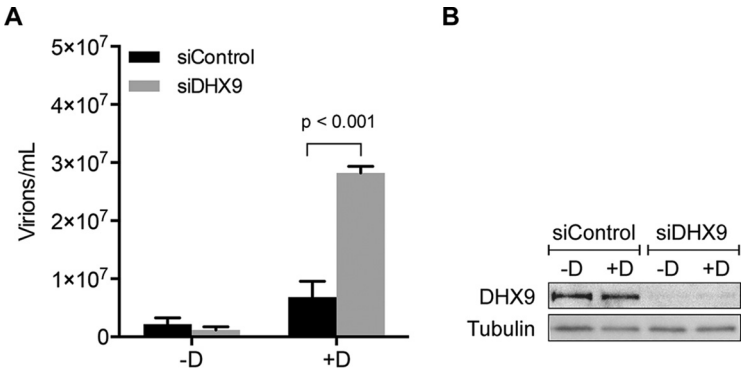

FIG 2 Effects of DHX9 depletion on EBV virion production. AGSiZ cells were depleted of DHX9 by siRNA transfection or mock depleted with control siRNA, followed by treatment with doxycycline (+D) to induce viral lytic replication or untreated (−D). (A) Quantification of infectious virus particles. Serial dilutions of virus-containing supernatant harvested at 5 days postinduction were used to infect 293T cells, and the number of GFP-positive cells representing infectious viral particles was measured by flow cytometry. Three independent biological experiments were performed, and each sample was measured in technical triplicates. (B) Knockdown efficiency of siDHX9. Protein cell lysates were harvested at 48 h after siRNA transfection and analyzed by Western blotting with anti-DHX9 antibody. The blot was stripped and reprobed with antitubulin antibody as a loading control.

SM expression construct in which lysates were immunoprecipitated with anti-DHX9 antibody. Consistent with the former experiment, SM was precipitated with DHX9 protein (Fig. 1C, lane 3). The control groups that were either transfected with empty vector or immunoprecipitated with control antibody showed no significant binding (Fig. 1C, lanes 1, 2, and 4).

Since DHX9 is known to contain RNA-binding motifs and to interact with RNA *in vivo*, we wished to ask whether the interaction between SM and DHX9 was RNA dependent. We therefore determined whether the SM-DHX9 interaction was RNase sensitive. 293T cells were transfected with SM expression plasmid, and lysates were harvested 48 h after transfection. Protein lysates were immunoprecipitated with anti-DHX9 antibody or control antibody and then treated or mock treated with RNase. After washing and elution, the immunoprecipitates were analyzed by immunoblotting with anti-SM antibody. RNase-treated and RNase-untreated samples exhibited similar amounts of SM coimmunoprecipitated with DHX9 (Fig. 1D, lanes 1 and 3). The result indicates that the majority of association between SM and DHX9 is RNase resistant and therefore not mediated by RNA bridging.

Effects of DHX9 depletion on infectious EBV virion production. We next investigated the functional importance of the interaction between SM and DHX9. Since SM is critical for EBV lytic gene expression (11, 41) and DHX9 is involved in the replication of many viruses, we hypothesized that a change in DHX9 expression might affect the level of EBV virion production. To explore the effect of DHX9 depletion on EBV infection, we used DHX9 small interfering RNA (siRNA) to knock down the cellular expression of DHX9. Experiments were performed in green fluorescent protein (GFP)-EBV-infected AGS gastric carcinoma cells which were transduced with a lentivirus expressing EBV transactivator Zta protein to generate an inducible cell line (AGSiZ) which synchronously and efficiently permits EBV lytic replication when treated with doxycycline (41). AGSiZ cells were depleted of DHX9 or mock depleted by control siRNA transfection followed by treatment with doxycycline to induce viral lytic replication or mock induced. Virus-containing supernatants were harvested 5 days postinduction, and serial dilutions of supernatant were used to infect uninfected 293T cells. The number of GFP-positive 293 cells, which is a quantitative measurement of infectious viral particles, was measured by flow cytometry 2 days later after infection as previously described (41). DHX9 depletion led to a 4-fold increase in infectious EBV titer in the supernatant (Fig. 2A) compared to induced cells transfected with control siRNA. Western blotting was performed to determine the knockdown efficiency of DHX9 siRNAs. Both unin-

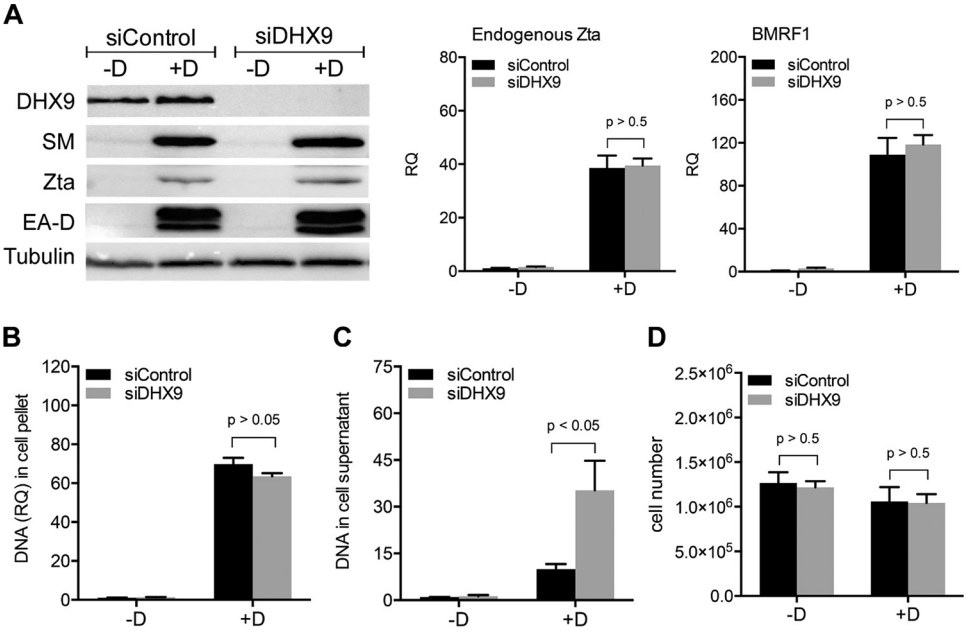

FIG 3 Effects of DHX9 depletion on EBV lytic gene expression, DNA replication, and extracellular virion release. AGSiZ cells were depleted of DHX9 or mock depleted by siRNA transfections, followed by treatment with doxycycline (+D) to induce viral lytic replication or untreated (−D). (A) Expression of EBV early and immediate early gene proteins and mRNAs. Protein lysates were harvested at 48 h postinduction and immunoblotted with anti-SM, anti-Zta, or anti-EA-D to examine the expression levels of EBV lytic genes. Blots were also probed with anti-DHX9 to confirm DHX9 knockdown and with antitubulin antibodies as a loading control. Transcript levels of endogenous Zta and BMRF1 were measured by qRT-PCR. (B) Quantification of intracellular EBV DNA. DNA was isolated from cell pellets harvested at 3 days postinduction and analyzed by qPCR. BILF2 primers were used to measure viral DNA (RQ, relative quantity). (C) Quantification of viral DNA in cell supernatant. Cell supernatants from cells treated as in panels A and B were harvested at 5 days postinduction for viral DNA isolation. Viral DNA quantities were measured by qPCR. (D) Quantitation of cell numbers after DHX9 knockdown. Three independent biological experiments were performed, and cell counts in each sample were measured in technical triplicates.

duced and induced siRNA-transfected cells showed efficient knockdown of DHX9 expression (Fig. 2B). Blots were probed with antitubulin antibody as a loading control. Our result indicates that knockdown of DHX9 results in increased EBV virion production, suggesting that DHX9 may act as an inhibitor of EBV lytic replication.

Effects of DHX9 depletion on EBV lytic gene expression and replication. Because depletion of DHX9 led to increased infectious EBV virion production, we performed further experiments to investigate which steps of the viral lytic cycle were affected by DHX9 knockdown. AGSiZ cells were depleted of DHX9 or mock depleted by siRNA transfection as described above, followed by treatment with doxycycline to induce lytic EBV replication or mock induction. In order to investigate whether EBV immediate early (IE) or early (E) gene expression was enhanced by DHX9 depletion and was contributing to the increase in viral infectious particles, we harvested siRNA-transfected cells 48 h after induction and measured EBV protein expression levels by Western blotting and gene transcript levels by qRT-PCR. Expression of EBV immediate early Zta protein and early proteins SM and EA-D was not affected by DHX9 depletion, and transcript levels of endogenous Zta and BMRF1 were not changed when DHX9 was depleted (Fig. 3A). These results suggested that DHX9 may act at steps after IE and E gene expression. We next measured the potential effect of DHX9 on EBV lytic DNA replication. AGSiZ cells were treated as previously and then harvested 3 days postinduction when DNA copy number is significantly increased by lytic DNA replication. DNA was isolated from cell pellets and analyzed by qPCR to measure the relative EBV DNA quantity. As shown in Fig. 3B, induction of replication led to an approximately 60-fold increase in EBV DNA levels. However, knockdown of DHX9 did not measurably affect lytic EBV DNA replication. This suggests that enhanced EBV DNA replication is not the

cause of increased EBV virion production when DHX9 is depleted but rather that other steps subsequent to DNA replication may be inhibited by DHX9. In order to ask whether increased numbers of infectious virions were released upon DHX9 depletion, we measured extracellular virion numbers after DHX9 knockdown. DNA was isolated from virus-containing supernatants harvested at 5 days postinduction, and qPCR was performed to measure the relative EBV DNA copy number. Figure 3C shows that knockdown of DHX9 resulted in an approximately 3- to 4-fold increase in the quantity of EBV genomes released compared to mock-depleted cells, consistent with the increase in infectious virus titer. Cell numbers were counted at 5 days postinduction to investigate whether the increase of virions in the DHX9-depleted supernatant resulted from altered cell numbers. There was no significant change in cell counts when DHX9 was depleted in cells undergoing lytic EBV replication (Fig. 3D). In summary, increased EBV infectious virion production mediated by DHX9 depletion is not due to enhanced viral IE or E gene expression and DNA replication but due to increased production of EBV virions.

DHX9 depletion leads to increased EBV late gene transcript levels. As described above, based on DHX9 knockdown, the inhibitory effects of DHX9 on EBV replication appeared to operate at a step subsequent to DNA replication. These steps in virion formation, including encapsidation, egress, and release, are dependent on EBV late gene proteins. Further, expression of 15 late genes is highly dependent on SM protein (11). Since DHX9 binds to SM, and SM interacts with its target viral mRNAs, it was possible that DHX9 was inhibiting SM function by sequestering it or interfering with its function. If this were the mechanism by which DHX9 inhibits EBV virion production, one would expect a preferential reduction in levels of SM-dependent late gene mRNAs. In order to test this hypothesis, we compared levels of representative SM-dependent and SM-independent genes under conditions of DHX9 depletion.

To measure the effects of DHX9 knockdown on viral late gene transcripts, we performed the following experiment in AGSiZ cells. Cells were depleted of DHX9 or mock depleted by siRNA transfections followed by treatment with doxycycline to induce viral lytic replication. Transfected cells were also mock induced in parallel to serve as a control for baseline expression of EBV mRNAs. Cells were harvested, and RNA was isolated 48 h after induction. RNA was analyzed by qPCR with 14 sets of viral late gene primers—7 sets for SM-dependent genes (BILF2, BDLF1, BDLF2, BZLF2, BcLF1, BLLF1, and BCRF1) and 7 sets for SM-independent genes (BFRF1, BFRF3, BORF1, BXLF2, BXRF1, BVRF2, and BBRF2)—to determine whether DHX9 effects on late gene transcripts operated in an SM-dependent or independent manner. Glyceraldehyde-3-phosphate dehydrogenase (GAPDH) was used as the endogenous cellular control. DHX9 depletion led to a 3-fold increase in lytic transcript levels regardless of whether the genes were SM dependent or independent (Fig. 4A and B). These data indicate that DHX9 has negative effects on late gene mRNA expression but that these effects are not mediated via SM function. The viral preinitiation complex (vPIC) is composed of six EBV proteins including BcRF1 (the viral TBP-like protein), which are necessary and sufficient for transcription of late viral genes (42, 43). In addition, the viral kinase BGLF4 is also required for efficient late gene expression (44). RNA was analyzed by qPCR with primers for these six genes (BGLF3, BDLF3.5, BcRF1, BFRF2, BVLF1, and BDLF4) and BGLF4 to determine whether any of the early lytic EBV genes specifically required for late gene transcription are affected by DHX9 knockdown. Modest increases were observed in the transcript levels of BGLF3, BcRF1, and BGFL4 when DHX9 was depleted (Fig. 4C and D). BGLF3 and BGLF4 have been shown to be necessary for expression of late genes as knockdown of BGLF3 or BGLF4 selectively abolished expression of late genes independent of any effect on expression of early genes or viral DNA replication (44). Moreover, BcRF1 encodes a TBP-like protein that binds TATT motifs found at EBV late gene promoters, and this interaction is required for activation of late viral gene expression (45). The modest induction of these vPIC genes may therefore contribute to the global increases in EBV late gene transcript abundance caused by DHX9 depletion.

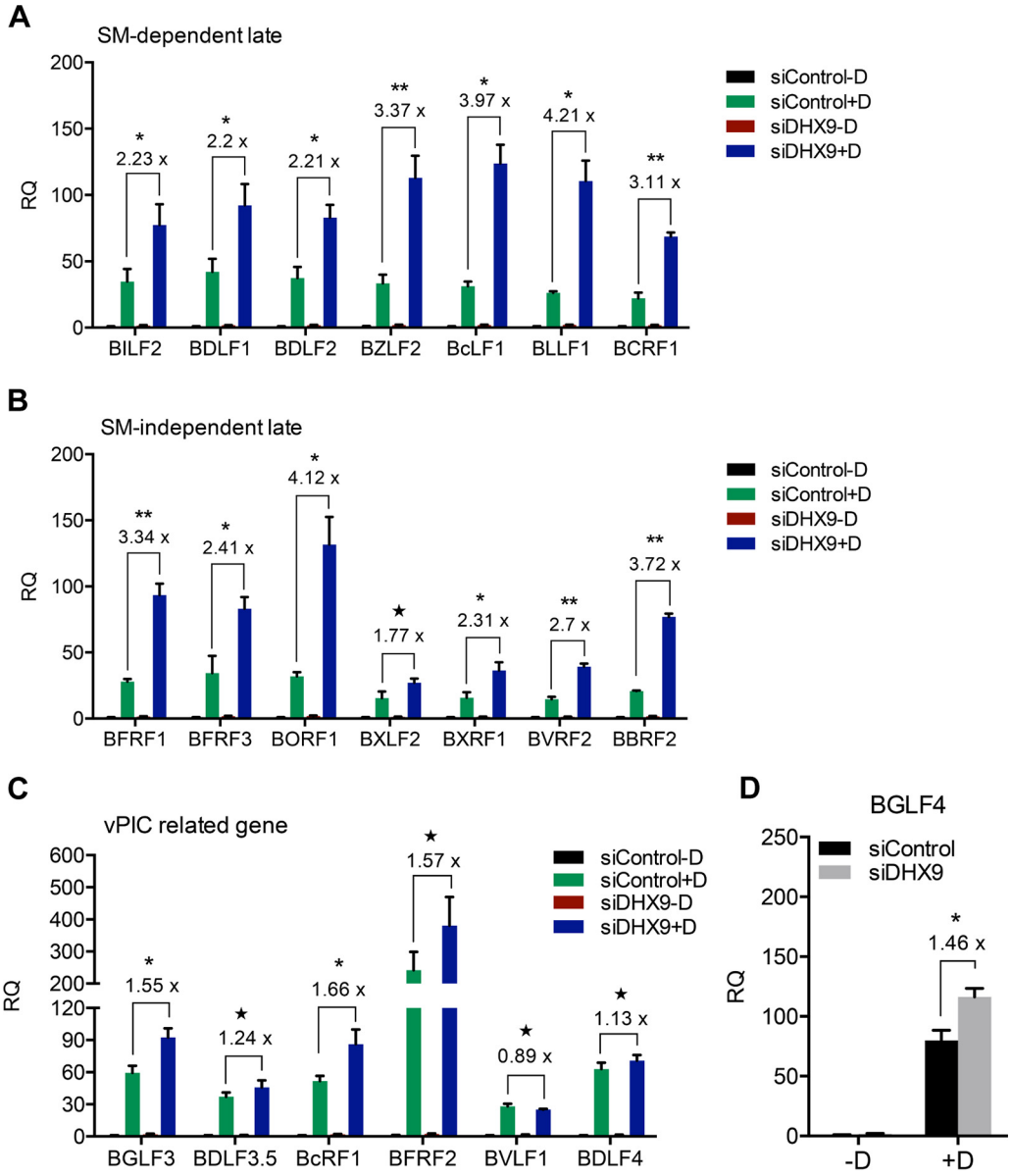

FIG 4 Effects of DHX9 depletion on EBV late gene transcript levels. AGSiZ cells were depleted of DHX9 or mock depleted by siRNA transfections followed by treatment with doxycycline (+D) to induce viral lytic replication or untreated (−D). Specific mRNA transcripts were measured by qRT-PCR with 7 sets of SM-dependent viral late gene primers (BILF2, BDLF1, BDLF2, BZLF2, BcLF1, BLLF1, and BCRF1) (A) and 7 sets of SM-independent late gene primers (BFRF1, BFRF3, BORF1, BXLF2, BXRF1, BVRF2, and BBRF2) (B) at 48 h postinduction. Transcript levels of vPIC-related genes (BGLF3, BDLF3.5, BFRF2, BcRF1, BVLF1, and BDLF4) (C) and BGLF4 (D) were measured by qRT-PCR. Three independent biological experiments were performed, and each sample was measured in technical triplicates. RQ, relative quantity. Fold changes of lytic transcript levels after DHX9 knockdown compared to control knockdown are shown above each gene. *, $P < 0.05$; **, $P < 0.001$; ★, $P > 0.05$.

As described above, DHX9 depletion by siRNA transfection increased EBV late gene transcript abundance and infectious viral particle production. Given the propensity of RNA interference (RNAi) to potentially have off-target effects, we used an additional unrelated DHX9 siRNA (siDHX9 #06) to repeat these experiments and verify these findings. As shown in Fig. 5A, DHX9 depletion by transfecting siDHX9 #06 led to a 3-fold increase in EBV virion production. No obvious change in transcript abundance or protein levels of early genes was observed (Fig. 5B). Knockdown of DHX9 did not measurably affect lytic EBV DNA replication (Fig. 5C), while a 2-fold increase in extracellular EBV DNA was observed when DHX9 was depleted by siDHX9 #06 transfection

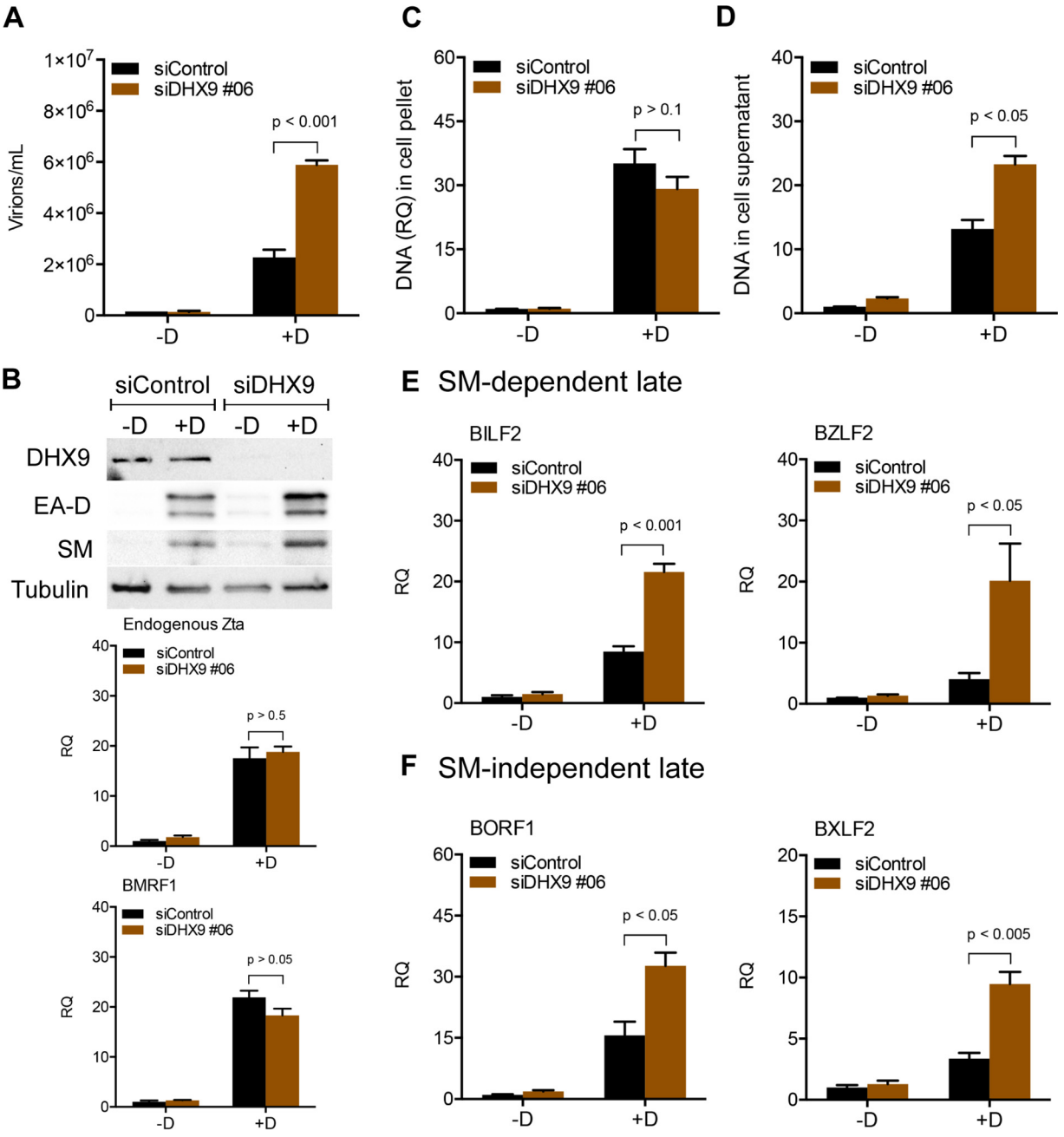

FIG 5 Effects of DHX9 depletion with second independent siRNA (siDHX9 #06) on EBV gene expression and virion production. AGSiZ cells were depleted of DHX9 or mock depleted by DHX9 siRNA transfections followed by treatment with doxycycline (+D) to induce viral lytic replication or untreated (−D). (A) Quantification of infectious virus particles. Serial dilutions of virus-containing supernatant harvested at 5 days postinduction were used to infect 293T cells, and the number of GFP-positive cells representing infectious viral particles was measured by flow cytometry. (B) Expression of EBV early and immediate early genes. (C) Quantification of intracellular EBV DNA. DNA was isolated from cell pellets harvested at 3 days postinduction and analyzed by qPCR. BILF2 primers were used to measure viral DNA (RQ, relative quantity). (D) Quantification of viral DNA in cell supernatant. Cell supernatants from cells treated as in panels A and B were harvested at 5 days postinduction for viral DNA isolation. Viral DNA quantities were measured by qPCR. (E and F) Quantification of SM-dependent (E) or SM-independent (F) EBV late gene transcripts by qRT-PCR. Three independent biological experiments were performed, and each sample was measured in technical triplicates.

(Fig. 5D). Moreover, DHX9 knockdown also had positive effects on EBV late gene transcripts generally, not specifically dependent on SM function. These results were all consistent with experiments described above performed with different siRNAs, confirming the specificity of effects observed with DHX9 depletion.

Effects of DHX9 depletion on EBV late gene expression, DNA replication, and virion production in HEK293-2089 cells. All of the above experiments were per-

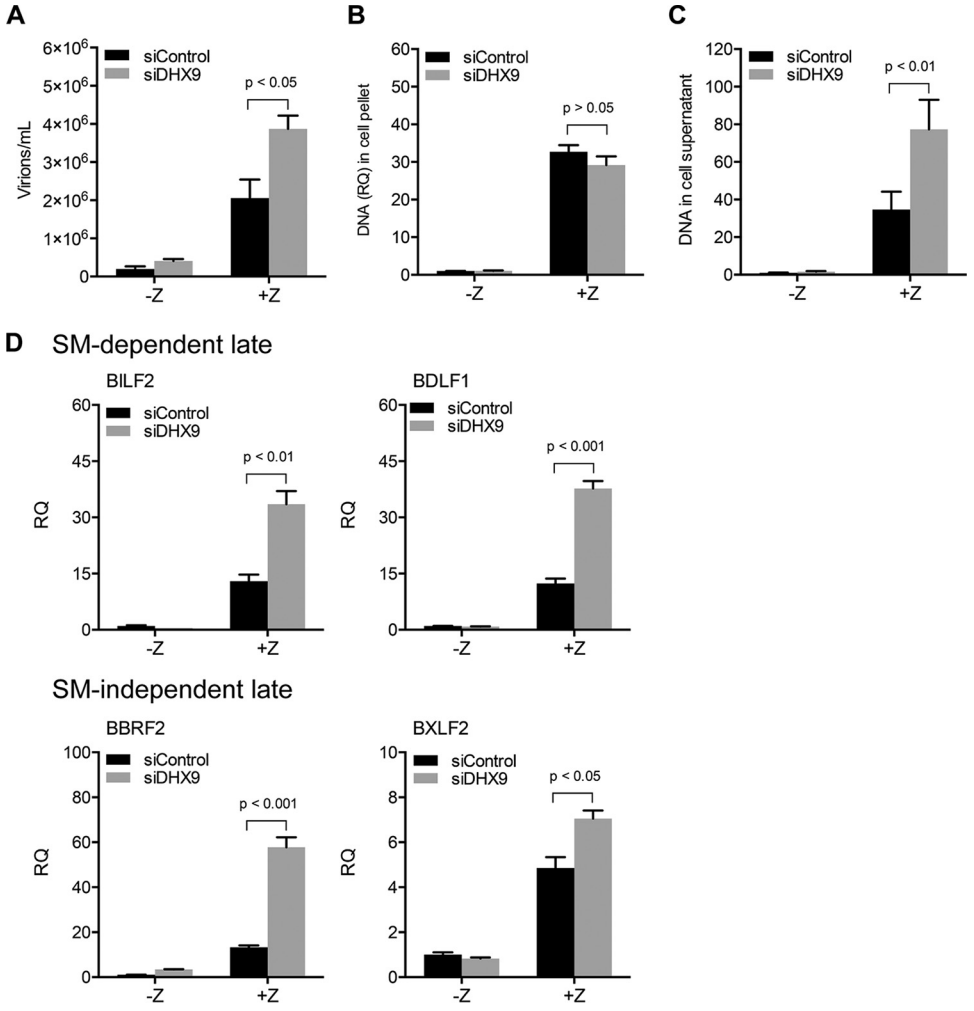

FIG 6 Effects of DHX9 depletion on EBV gene expression and virion production in HEK293-2089 cells. HEK293-2089 cells were depleted of DHX9 or mock depleted by siRNA transfections followed by transfection with transactivator plasmid Zta (+Z) to induce viral lytic replication or transfected with empty vector (−Z). (A) Quantification of infectious virus particles. Serial dilutions of virus-containing supernatant harvested at 5 days postinduction were used to infect 293T cells, and the number of GFP-positive cells representing infectious viral particles was measured by flow cytometry. (B) Quantification of intracellular EBV DNA. DNA was isolated from cell pellets harvested at 3 days postinduction and analyzed by qPCR. BILF2 primers were used to measure viral DNA (RQ, relative quantity). (C) Quantification of viral DNA in cell supernatant. Cell supernatants from cells treated as in panels A and B were harvested at 5 days postinduction for viral DNA isolation. Viral DNA quantities were measured by qPCR. (D) Quantification of EBV SM-dependent and SM-independent late gene transcripts by qRT-PCR. Three independent biological experiments were performed, and each sample was measured in technical triplicates.

formed in Zta-inducible, EBV Akata-positive gastric carcinoma cell line AGS (AGSiZ) (41). In order to eliminate the possibility that the phenotype of DHX9 knockdown was due to effects on the performance of the Zta-inducible system, we repeated DHX9 depletion experiments in HEK293-2089 cells infected with EBV. Zta plasmid was transfected to induce viral lytic replication. Virus-containing supernatants were harvested 5 days postinduction, and serial dilutions of supernatant were used to infect 293T cells to measure viral infectious particles as previously performed. DHX9 depletion led to an approximately 2-fold increase in virion production (Fig. 6A). DNA was isolated from cell pellets at 3 days postinduction and analyzed by qPCR to measure the relative EBV DNA quantity. As shown in Fig. 6B, knockdown of DHX9 did not measurably affect lytic EBV DNA replication. DNA was isolated from virus-containing supernatants harvested at 5 days postinduction to measure extracellular virion numbers after DHX9 knockdown by qPCR (Fig. 6C). DHX9 depletion resulted in an approximately 2-fold increase in the quantity of EBV genomes released compared to mock-depleted cells. Cells were

harvested, and RNA was isolated 48 h after induction. RNA was analyzed by qPCR with 4 sets of viral late gene primers, BILF2, BDLF1, BBRF2, and BXLF2, to determine the effects of DHX9 depletion on EBV late gene transcripts. GAPDH was used as the endogenous cellular control. DHX9 depletion led to a 2- to 3-fold increase in lytic transcript levels regardless of whether the genes were SM dependent or independent (Fig. 6D). All these results were consistent with those in AGSiZ cells. These demonstrate that increased late gene expression and virion production caused by DHX9 knockdown were not due to the effects of DHX9 depletion on the performance of the Zta-inducible system.

DHX9 colocalizes with SM in cells undergoing lytic EBV replication. Since SM interacted with DHX9, we asked whether the two proteins would colocalize in the nucleus. We performed immunofluorescence (IF) studies in EBV-infected cells: AGSiZ, HEK293-2089, and SMKO 293 cells. AGSiZ cells were treated with doxycycline to induce viral lytic replication, and HEK293-2089 (293 cells infected with the B95-8 2089 bacmid) cells were transfected with Zta plasmid to induce viral lytic replication; 48 h postinduction, cells were fixed and costained for DHX9 and SM and visualized by fluorescence microcopy. A similar experiment was performed in SMKO cells (293 cells infected with an SM-negative EBV recombinant, BMLF1KO) (5, 6), except that cells were cotransfected with both Zta and SM plasmids. As shown in Fig. 7A, DHX9 was found to highly but not completely colocalize with SM in the nuclei. In order to define the interaction between SM and DHX9, we performed a colocalization analysis with ImageJ-plot profile to display a two-dimensional graph of the intensities of pixels along the longitudinal axis within cells in merged images (Fig. 7B). The *x* axis represents the distance along the longitudinal cell axis, and the *y* axis is the pixel intensity for each fluorophore. DHX9 and SM primarily shared the same locations in cells, even though they had differences in pixel intensity. These data suggest that DHX9 highly colocalizes with SM and primarily in the nucleus. Immunoblotting was performed to compare levels of DHX9 protein in SM-expressing and nonexpressing cells, to assess the effects of SM on DHX9 protein expression. As shown in Fig. 7C, the total protein levels of DHX9 did not change appreciably in SM-expressing cells.

Effects of DHX9 depletion on type I interferon pathway and interferon expression in EBV-infected cells. Although DHX9 has been demonstrated to act as a proviral factor enhancing viral replication in many systems, it has also been implicated as a restrictive factor for herpes simplex virus (HSV), influenza virus, and myxoma virus, where it may play a role as a sensor of nucleic acids to activate an antiviral response (22, 39) We therefore asked whether depletion of DHX9 led to decreased expression of innate immune effector molecules in EBV-infected cells that could explain DHX9 effects on EBV lytic replication. AGSiZ cells were depleted of DHX9 or mock depleted by siRNA transfection. Cells were harvested, and RNA was isolated 48 h after DHX9 knockdown (KD) and analyzed by high-throughput sequencing. We examined differential cellular gene expression between DHX9-depleted and mock-depleted AGSiZ cells. Three hundred twenty cellular genes which were downregulated at least 2-fold ($\log_2$ fold change ≤ -1) by DHX9 KD were subjected to gene ontology (GO) analysis. Functional annotation of genes was based on GO (http://www.geneontology.org), and enrichment analysis (overrepresentation) was performed to identify GO categories that might be enriched in the downregulated genes. As shown in Table 1, several processes related to the type I interferon signaling pathway, negative regulation of viral genome replication, and defense response to virus were significantly downregulated in the DHX9-depleted cells compared to mock-depleted cells. A list of genes enriched in these biological processes is shown in Table 2. No other pathways were identified by the ontology analysis. We performed qRT-PCR to measure mRNA abundance of several interferon-stimulated genes (ISGs) which were downregulated at least 2-fold when DHX9 was depleted to further validate these results. Transcript levels of IFIT5, OAS3, IFIT3, OAS1, OAS2, and IFIT1 were significantly decreased when DHX9 was depleted (Fig. 8A and B). We then investigated the changes of these genes when DHX9-depleted

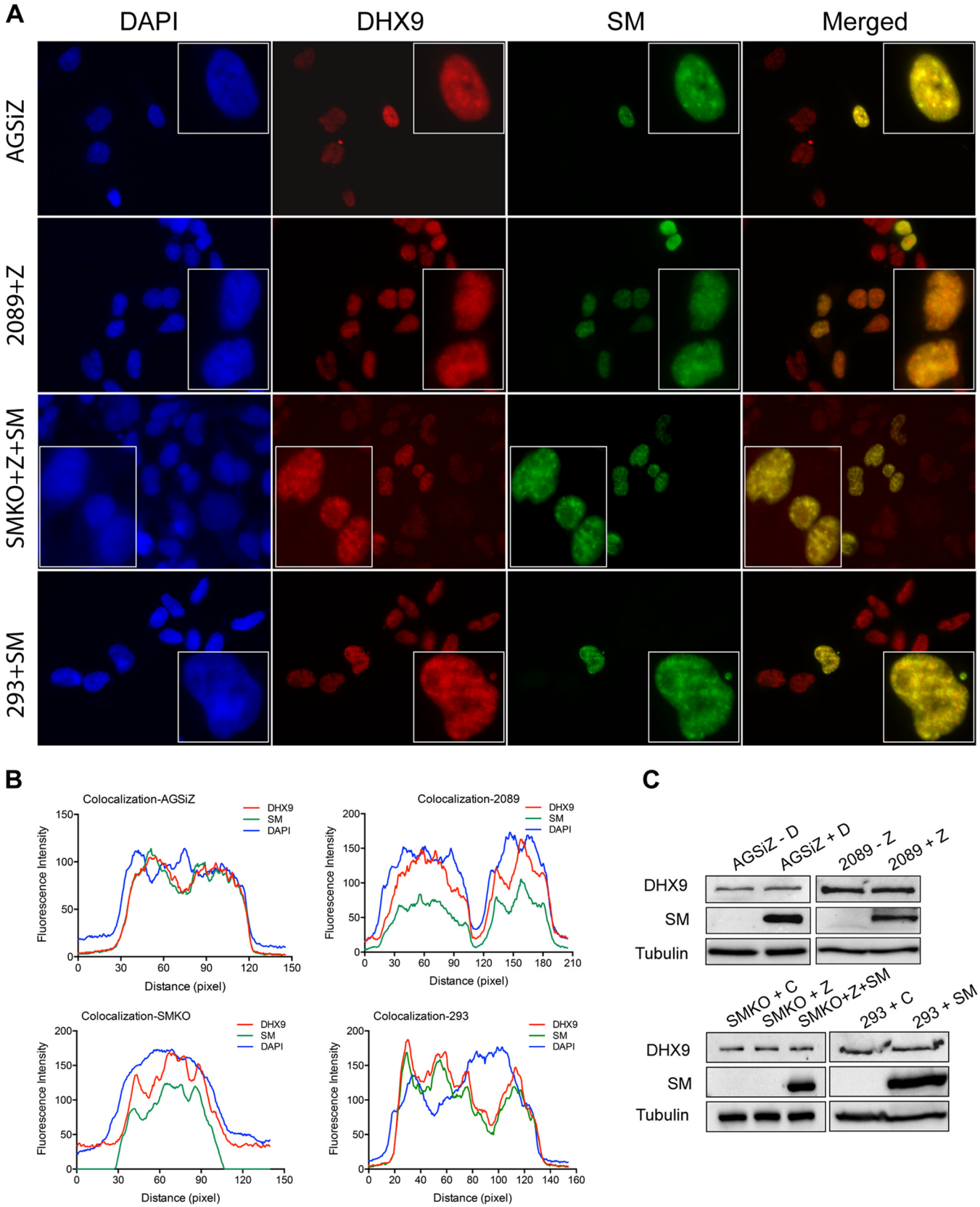

FIG 7 DHX9 colocalizes with SM in various cell lines. (A) Localization of DHX9 and SM in AGSiZ, HEK2089, SMKO, and HEK293 cells. AGSiZ cells were treated with doxycycline (+D) to induce viral lytic replication; 2089 cells were transfected with plasmid Zta to induce viral lytic replication; SMKO cells were cotransfected with Zta and SM to induce lytic replication; uninfected HEK293 cells were transfected with untagged SM plasmid. At 48 h postinduction, cells

(Continued on next page)

AGSiZ cells were induced to permit lytic replication. As shown in Fig. 8C and D, OAS1, IFIT1, OAS3, and MX1 were found to be downregulated by DHX9 knockdown, even when cells were undergoing lytic replication. These suggest that decreased expression of innate immune effectors by DHX9 depletion may result in the increased EBV virion production observed.

DHX9 is known to enhance NF-κB-mediated transcriptional activation by p65 through its functional NTPase/helicase activity (46), and knockdown of DHX9 expression blocks the ability of myeloid dendritic cells (DCs) to produce type I IFN and proinflammatory cytokines in response to virus infection (22, 30). Type I interferon (IFN) is a key component of the innate immune response against virus infections (47). Type I IFN is known to block HSV replication at an early step in replication and to be important for resistance against viral infection (48, 49). It was therefore possible that DHX9 exerted its effects on the antiviral response via upregulation of type I IFN. In order to ask whether the observed changes in gene expression upon DHX9 KD were due to IFN upregulation by DHX9, we examined the transcript levels of IFN-β in AGSiZ cells that were transfected with either control siRNAs or DHX9 siRNAs and either induced or mock induced to permit EBV replication as in Fig. 4 above. As shown in Fig. 8E, the transcript levels of IFN-β were only slightly decreased by DHX9 depletion, in both EBV-induced and EBV-uninduced cells. These results suggest that DHX9 may enhance the antiviral response but may not act primarily via stimulation of IFN synthesis because the effects on the subset of ISGs affected were markedly greater than the effects on IFN levels.

In order to confirm that activation of IFN pathways would have the expected antiviral effect against EBV, we treated AGSiZ cells with various doses of IFN-β and induced viral lytic replication with doxycycline. Virus-containing supernatants were harvested 5 days postinduction, and serial dilutions of supernatant were used to infect 293T cells to measure infectious virus particle production (Fig. 8F). Virion production was decreased when cells were treated with IFN-β in a dose-dependent manner. RNA was harvested and isolated to be measured by qPCR with EBV late gene BZLF2 primers. Consistent with virion production data, EBV late gene transcript level was decreased by IFN-β treatment, in a dose-dependent manner (Fig. 8G).

SM expression leads to decreased CREB transcriptional activity. Since the antiviral effect of DHX9 appeared to be unrelated to an effect on SM, we asked whether SM might counteract DHX9, thereby acting as a viral antagonist to a host defense mechanism. DHX9 has been shown to interact with the CREB-binding protein (CBP), bridging CBP and holo-RNA polymerase II complexes, and to be required for DHX9-mediated transcriptional activation (50). We asked whether SM could inhibit this known function of DHX9. We used the pCRE Tluc16-DD plasmid, a transcriptional reporter plasmid designed to monitor the activation of cAMP-binding protein (CREB) and cAMP-mediated signal transduction pathways in mammalian cells (51). In HEK293 cells, we either depleted DHX9 expression by siRNA transfection or overexpressed DHX9 by transfecting FLAG-tagged RHA expression plasmid. Thirty hours later, cells were transfected with pCRE Tluc16-DD reporter vector. At 24 h posttransfection, cells were harvested and lysates were prepared for luciferase assays and Western blotting. A reduction of CREB luciferase activity was observed in DHX9-depleted cells in Fig. 9A, whereas luciferase activity was slightly increased when DHX9 was overexpressed (Fig. 9B), demonstrating that DHX9 could regulate CREB promoter-luciferase reporter activity. We then tested the effect of SM expression in this system. HEK293 cells were cotransfected with SM expression plasmid or empty vector and pCRE Tluc16-DD

FIG 7 Legend (Continued)
were costained for DHX9 (red) and SM (green) and visualized by fluorescence microcopy. The nuclei were stained with DAPI (blue). (B) Colocalization analysis with ImageJ of cells shown in the boxes as in panel A. Two-dimensional graph of the intensities of pixels along the longitudinal axis of cells in merged images. The *x* axis represents distance along the line, and the *y* axis is the pixel intensity. (C) Expression of DHX9 and SM in AGSiZ, 2089, SMKO, and 293 cells. Protein cell lysates were harvested at 48 h postinduction and analyzed by Western blotting with anti-DHX9 and anti-SM antibodies. Tubulin was probed as a loading control.

TABLE 1 Gene ontology enrichment analysis for cellular genes downregulated by DHX9 depletion (log_2 fold change <-1)

GO biological process complete	*Homo sapiens* (reference) no.	No.	Expected	Fold enrichment	+/−	*P* value[a]
Type I interferon signaling pathway (GO:0060337)	66	13	1.04	12.56	+	2.06E−06
↳ Cellular response to type I interferon (GO:0071357)	66	13	1.04	12.56	+	2.06E−06
↳ Response to type I interferon (GO:0034340)	71	13	1.11	11.68	+	4.56E−06
Negative regulation of viral genome replication (GO:0045071)	53	9	0.83	10.83	+	3.85E−03
↳ Regulation of viral genome replication (GO:0045069)	89	10	1.4	7.16	+	2.70E−02
Defense response to virus (GO:0051607)	191	21	3	7.01	+	1.47E−07
↳ Defense response to other organism (GO:0098542)	515	24	8.08	2.97	+	3.37E−02
↳ Response to other organism (GO:0051707)	949	36	14.88	2.42	+	1.53E−02
↳ Response to external biotic stimulus (GO:0043207)	951	36	14.91	2.41	+	1.59E−02
↳ Response to biotic stimulus (GO:0009607)	977	36	15.32	2.35	+	4.13E−02

[a]Displaying only results for Bonferroni-corrected value for $P < 0.05$.

reporter vector. At 24 h posttransfection, cells were harvested and lysates were prepared for luciferase assays and Western blotting. A significantly decreased luciferase activity was observed in SM-expressing cells compared to cells without SM expression (Fig. 9C), demonstrating that SM is capable of inhibiting CREB-mediated transcriptional activation. In sum, these data suggest that SM may inhibit DHX9-mediated CREB-dependent transcriptional activation.

DISCUSSION

EBV SM protein is a nuclear protein essential for EBV lytic replication and has functional roles in mRNA stabilization, splicing, export, and translation (5–10, 12–17). We have shown that SM specifically enhances expression of a subset of EBV late genes whose expression is highly SM dependent and which are critical for virion formation and infectivity (11). SM also associates with cellular splicing factor SRp20, alters splicing of cellular STAT1 mRNA, and changes the pattern of STAT1 expression to potentially modulate host innate immune responses during EBV reactivation and lytic replication (9). In previous studies, we discovered functional links between SM and cellular proteins such as Sp110b and SRp20 after identifying the SM-interacting proteins by mass spectrometry (9, 12). Since DHX9 (RNA helicase A [RHA]) was also identified as a major cellular SM-binding protein, we investigated the functional consequences of this interaction on EBV replication.

TABLE 2 List of genes enriched in the biological processes shown in Table 1

Gene ID	Gene name	Type I interferon signaling pathway	Negative regulation of viral genome replication	Defense response to virus
TRIM34	Tripartite motif-containing protein 34			X
IFIT5	Interferon-induced protein with tetratricopeptide repeats 5		X	X
IRF9	Interferon regulatory factor 9	X		X
RNASE6	RNase K6			X
IFI27	Interferon alpha-inducible protein 27, mitochondrial	X	X	X
RSAD2	Radical *S*-adenosylmethionine domain-containing protein 2	X	X	X
IFIT3	Interferon-induced protein with tetratricopeptide repeats 3	X		X
DHX58	Probable ATP-dependent RNA helicase DHX58			X
SPON2	Spondin-2			X
BST2	Bone marrow stromal antigen 2	X	X	X
OAS1	2′-5′-Oligoadenylate synthase 1	X	X	X
IFI16	Gamma-interferon-inducible protein 16			X
IFI44L	Interferon-induced protein 44-like			X
DDX58	Probable ATP-dependent RNA helicase DDX58			X
IFI6	Interferon alpha-inducible protein 6	X	X	X
OAS3	2′-5′-Oligoadenylate synthase 3	X	X	X
MX2	Interferon-induced GTP-binding protein Mx2	X		X
AC093510	DNA-directed RNA polymerase III subunit RPC7	X		X
IFIT1	Interferon-induced protein with tetratricopeptide repeats 1	X	X	X
OAS2	2′-5′-Oligoadenylate synthase 2	X		X
ISG15	Ubiquitin-like protein ISG15	X	X	X

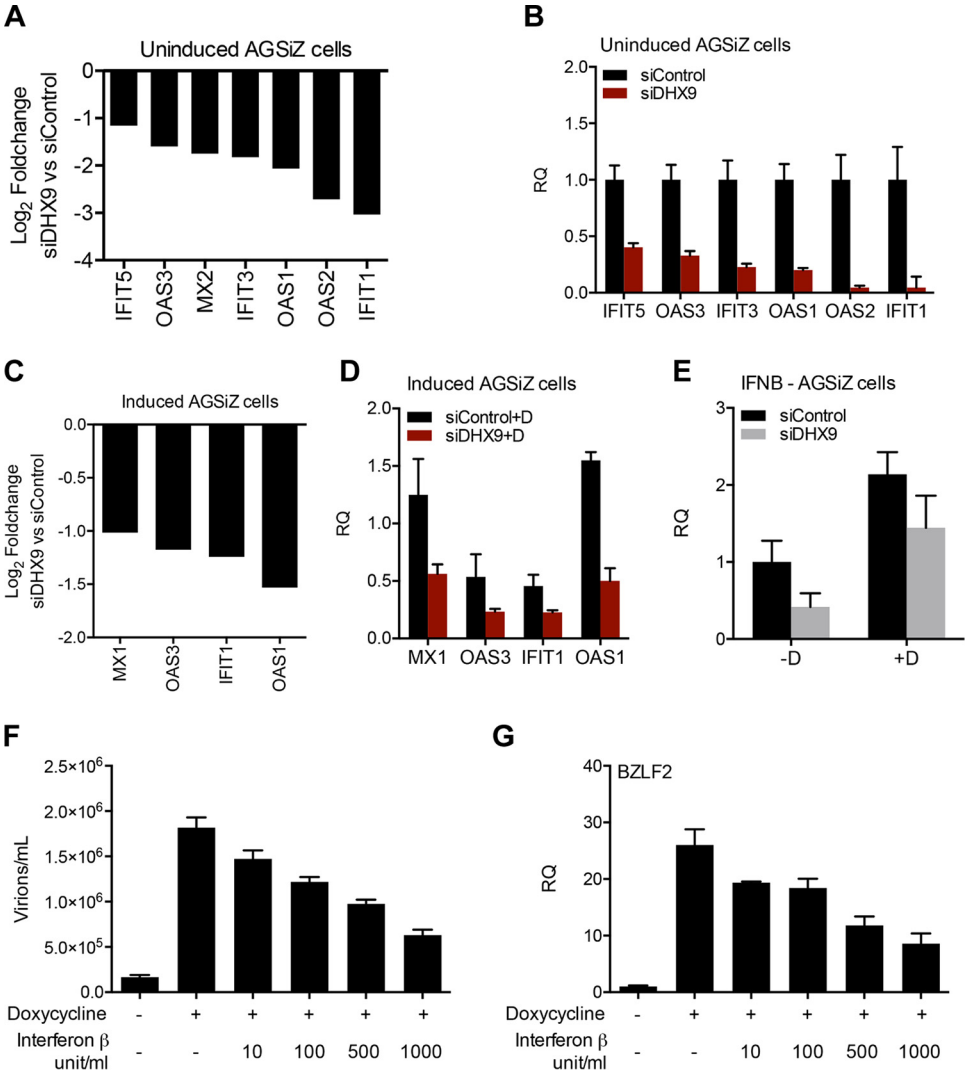

FIG 8 Effect of DHX9 depletion on type I interferon pathway and IFN-β expression. (A to D) Effect of DHX9 KD on ISG expression. AGSiZ cells were depleted of DHX9 or mock depleted by siRNA transfection followed by treatment with doxycycline (+D) to induce viral lytic replication or left untreated (−D). RNA was harvested at 48 h postinduction and analyzed by high-throughput sequencing and by qRT-PCR. (A) Log_2 fold changes of selected interferon-stimulated genes after DHX9 depletion of uninduced AGSiZ cells derived from differential expression of RNA-seq data. (B) ISG mRNA levels of genes shown in panel A were quantitated by qRT-PCR. (C) Log_2 fold changes of selected interferon-stimulated genes after DHX9 depletion of induced AGSiZ cells derived from differential expression of RNA-seq data. (D) ISG mRNA levels of genes shown in panel C were quantitated by qRT-PCR. (E) Effect of DHX9 depletion on IFN-β transcript levels. RNAs from experiments above were analyzed by qPCR with primers specific for IFN-β. (F and G) Dose-dependent effects of IFN-β treatment on EBV lytic virion production and late gene transcripts. Various concentrations of IFN as shown were added to the medium of AGSiZ cells when doxycycline was added to induce viral lytic replication. At 5 days postinduction, virus-containing supernatant was harvested and released infectious viral particles were quantitated as described above (F). Total RNA was isolated from cell pellets at 48 h postinduction, and late gene expression was measured by qRT-PCR (G). GAPDH was used as the endogenous control. RQ, relative quantity. Three independent biological experiments were performed, and each sample was measured in technical triplicates.

DHX9 is a multifunctional ATP-dependent nucleic acid helicase that unwinds DNA and RNA in a 3′ to 5′ direction and is involved in many cellular processes involving RNA, such as transcriptional activation, posttranscriptional RNA regulation, splicing, mRNA translation, and RNA-mediated gene silencing (46, 51–54). DHX9 has been reported to promote infectivity of various viruses, including HIV, retrovirus, influenza virus, and foot-and-mouth disease virus (FMDV). DHX9 binds (via DRBM domain 2) to the HIV-1 TAR RNA and stimulates HIV-1 transcription of transactivation response element (TAR)-containing mRNAs (21, 33). DHX9 also was found to regulate HIV-1 *gag* mRNA trans-

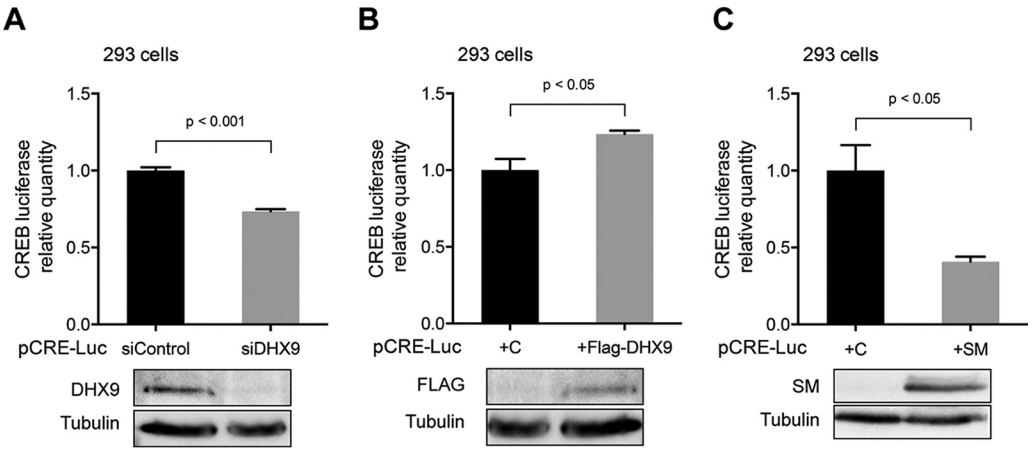

FIG 9 SM effect on transcription activation via the CRE. (A) Effect of DHX9 depletion on CRE-luciferase activity in HEK293 cells. HEK293 cells were depleted of DHX9 with siRNA or mock depleted with control siRNA. At 30 h post-siRNA transfection, cells were transfected with pCRE-luc reporter vector. At 24 h after transfection of the reporter, cells were lysed for luciferase assay and analyzed by Western blotting to examine the knockdown efficiency of DHX9. (B) Effect of DHX9 overexpression on CRE-luciferase activity. The pCRE-luc reporter vector was cotransfected with FLAG-tagged DHX9 expression plasmid or empty vector (C). At 24 h posttransfection, cells were harvested and lysed for luciferase assay. Protein lysates were analyzed by Western blotting to detect DHX9 overexpression. (C) Effect of SM expression on CRE-luciferase activity in HEK293 cells. The pCRE-luc reporter vector was cotransfected with SM plasmid or empty vector (C). At 24 h posttransfection, cells were harvested and lysates were prepared for luciferase assay. Protein lysates were analyzed by Western blotting to detect SM expression. All transfections were performed in triplicate, and technical triplicates of each sample were measured by luciferase assay.

lation by binding to a posttranscriptional control element (PCE) in the 5′ untranslated region (UTR) (55). In retroviruses that do not encode a Rev-like protein, DHX9 acts similarly to the retroviral Rev protein by mediating nuclear export of both CTE-containing (e.g., simian type D retrovirus) (31, 32) and RRE-containing (e.g., HIV-1) RNA (33). DHX9/RHA also enhances transcription and replication in the influenza virus life cycle (38).

In this study, we investigated the effects of DHX9 expression on EBV lytic replication. Surprisingly, we found that depletion of DHX9 led to a 4-fold increase in infectious EBV titer in the supernatant and a 3-fold increase in EBV late gene transcripts broadly. These data indicate that DHX9 has negative effects on EBV infectious virus production. Similar functions for DHX9 in myxoma virus (MYXV) replication were recently reported (39). DHX9 knockdown led to an increase in MYXV replication, suggesting that DHX9 may have potential antiviral functions. Our finding that DHX9 bound to SM protein, and the fact that SM is essential for efficient expression of a specific subset of late EBV transcripts (11), suggested that DHX9 might act by directly inhibiting SM function. However, the inhibitory effect of DHX9 on EBV mRNA accumulation was not confined to SM-dependent mRNAs but was evident on both SM-dependent and independent transcripts. We then considered whether the effects of DHX9 depletion on late gene expression were mediated by effects on the expression of the EBV viral preinitiation complex (vPIC) and BGLF4, which are crucial to EBV late gene transcription (42–45). DHX9 depletion was shown to induce a modest increase to the transcript levels of BGLF3, BcRF1, and BGFL4, but less than the global effect on late genes. This suggests that while the modest increases of vPIC-related genes and BGLF4 transcripts seen with DHX9 KD may contribute to enhanced EBV production, additional factors likely play a role.

DHX9 has been reported to function as a direct or indirect regulator in the activation of antiviral signaling pathways. DHX9 acts as a cytosolic MyD88-dependent viral DNA and RNA sensor in plasmacytoid dendritic cells (DCs), where knockdown of DHX9 expression dramatically blocked the ability of DCs to produce type I IFN and proinflammatory cytokines in response to dsRNA and RNA viruses (22). According to our transcriptome sequencing (RNA-seq) and GO analysis, 21 genes assigned to the bio-

logical processes of type I interferon signaling pathway, negative regulation of viral genome replication, and defense response to virus were found to be downregulated when DHX9 was depleted (Tables 1 and 2). Because DHX9 may contribute to type I IFN production by acting as an innate immune sensor and enhancing IFN mRNA synthesis (56), it was possible that these ISG effects were attributable to decreased IFN production in the absence of DHX9. However, IFN mRNA levels were not significantly decreased by DHX9 KD, suggesting that while DHX9 may play a role as a pathogen sensor under some conditions, it does not play a role in enhancing IFN production in the epithelial cell systems used in this study and does not affect all ISGs. Nevertheless, as shown by transcriptome analysis and qPCR, a specific subset of ISGs important for the antiviral response is highly dependent on DHX9. While the mechanisms by which DHX9 may affect cellular gene expression are numerous, it has been demonstrated that DHX9 may enhance transcription of ISGs in cells treated with interferon (56). Therefore, it is possible that the dependence of specific ISGs on DHX9 that we describe may be due to transcriptional effects of DHX9.

Our results indicate that transcriptional activation mediated by CREB was affected in the presence of SM. Several reports have established that DHX9 plays a role as a transcriptional coactivator, acting as a bridging factor between polymerase II holoenzyme and transcription factors or cofactors, such as BRCA1 and CREBBP (57). The CREB binding protein (CBP) stimulates gene transcription expression via its association with RNA polymerase II complexes (50). DHX9 helps recruit holo-RNA polymerase II to CBP and cooperates with CBP in mediating target gene activation via CREB (50). The ATPase and/or helicase activity of DHX9 is required for CREB-dependent transcription (51). Our finding that SM inhibits CREB-dependent transcription suggests that SM may interact with DHX9 and counteract its transcription-activating function. While we do not have direct evidence for SM directly antagonizing the transcriptional effects of DHX9, this work lays the basis for further research such as mutational analyses that disrupt the DHX9-SM interaction to determine if the DHX9-SM interaction represents another example of the virus-host arms race.

In summary, we report that depletion of the cellular helicase DHX9 enhances EBV virion production and expression of viral late gene transcripts, demonstrating that DHX9 is a cellular restriction factor for EBV. These effects were evident with both SM-dependent and independent genes, suggesting that the antiviral effect of DHX9 is not mediated by binding and inhibiting SM function. However, DHX9 enhanced innate antiviral pathways active against EBV but was not essential for IFN induction by EBV replication. Rather, DHX9 appears to have positive effects on expression of a subset of ISGs, allowing it to exert broad antiviral activity.

MATERIALS AND METHODS

Cells, plasmids, and transfection. AGSiZ is derived from the gastric carcinoma cell line AGS infected with GFP-expressing EBV Akata BX1 by stable transduction of a lentivirus expressing the EBV transactivator Zta under the control of a doxycycline-inducible promoter (41). AGSiZ cells were cultured in Ham's F-12 medium supplemented with 10% fetal bovine serum (FBS) and 1% GlutaMAX (Invitrogen) and selected with 0.5 mg/ml neomycin and 0.5 μg/ml puromycin. HEK293 cells stably carrying 2089 B95-8 EBV bacmid were maintained as monolayer cultures in Dulbecco's modified Eagle's medium supplemented with 10% FBS, 1% GlutaMAX supplement (Life Technologies), and 100 μg/ml of hygromycin (58). HEK293 cells carrying an SM-null EBV 2089 bacmid with the SM gene inactivated by insertion of a kanamycin resistance gene (EBV BMLF1^{KO}) (5), referred to as SMKO EBV, were maintained in parallel. Cells were all grown at 37°C, 5% CO_2. Plasmids F-SM, SM, BZLF1 (Zta), and BALF4 used in this study have been previously described (6, 10). The pCRE Tluc16-DD plasmid, a transcriptional reporter plasmid designed to monitor the activation of cAMP-binding protein (CREB) and cAMP-mediated signal transduction pathways in mammalian cells, was purchased from ThermoFisher. Transfections of 293 cells were performed with TransIT293 reagent (Mirus Bio) according to the manufacturer's protocol.

Protein affinity purification, silver staining, and mass spectrometry. 293T cells transfected with FLAG-tagged SM expression vector (F-SM) or empty vector were harvested at 48 h after transfection. SM complexes were purified from the cell lysates as follows. Cells were detached from plates with phosphate-buffered saline (PBS) containing EDTA, washed, and lysed in lysis buffer (50 mM Tris-HCl [pH 7.4], 1 mM EDTA, 1% Triton X-100) with mammalian protease inhibitor cocktail (Sigma), followed by incubation at 4°C with occasional mixing for 30 min, followed by sonication at 4°C. Lysates were clarified by centrifugation for 10 min at 12,000 $\times$ *g* and incubated for 2 h with anti-FLAG M2 antibody-conjugated

affinity gel (Sigma). The agarose matrix was washed extensively, and SM complexes were eluted with 150 μl of 1-mg/ml FLAG peptide in Tris-buffered saline, with shaking for 30 min at room temperature. Vector-transfected cells and SM-transfected cells were processed in parallel, and eluates were analyzed by SDS-PAGE and silver staining to assess recovery and purity. Silver staining was performed similarly to previous studies (9). Briefly, after electrophoresis, the gel slab was fixed in 50% methanol-5% acetic acid in water for 20 min. It was then washed with 50% methanol to remove the remaining acid. The gel was sensitized by a 1-min incubation in 0.02% sodium thiosulfate and rinsed with two changes of distilled water for 1 min each. After rinsing, the gel was submerged in chilled 0.1% silver nitrate solution and incubated for 20 min at 4°C. After incubation, the silver nitrate was discarded, and the gel slab was rinsed twice with water for 1 min and then developed in 0.04% formalin (35% formaldehyde in water [Merck, Darmstadt, Germany]) in 2% sodium carbonate with intensive shaking. After the desired intensity of staining was achieved, the development was terminated by with 5% acetic acid. Silver-stained gels were stored in a solution of 1% acetic acid at 4°C. Tandem mass spectrometry (MS/MS) analysis of protein complexes in solution or from excised gel slices was performed at the University of Florida ICBR Proteomics facility, and the data were analyzed by using Scaffold software as previously described (9).

Co-IP assay and RNase A treatment. Coimmunoprecipitation (co-IP) of DHX9 and SM was performed using HEK293 cells with SM overexpressed by transfecting FLAG-tagged or untagged SM plasmids. At 48 h posttransfection, cells were harvested and lysed in 200 μl ice-cold 1% NP-40 lysis buffer for 10 min. The lysed cell suspension was centrifuged for 30 min s at 10,000 $\times$ *g* at 4°C. The cleared supernatant was precleared with 2.5 μg rabbit immunoglobulin G (Bethyl), followed by incubation with protein A-conjugated agarose beads. The precleared samples were used for immunoprecipitation. Two micrograms of mouse monoclonal anti-FLAG antibody (Sigma), control IgG (Bethyl), or rabbit polyclonal anti-SM antibody was added to the lysate, followed by incubation for 1 h at 4°C. Immune complexes were incubated with 20 μl of either protein A-conjugated beads or protein G-conjugated beads for 2 h at 4°C. RNase treatment was performed with 100 μg of RNase A/ml for 30 min at 37°C. The beads were washed four times in wash buffer (Tris-buffered saline [pH 7.4], 500 mM NaCl, 1% Triton X-100) and then boiled for 5 min in SDS-PAGE loading buffer. Protein samples were stored at −20°C before use.

Western blot assay for viral proteins. Cell protein lysates were prepared and then separated on SDS-containing polyacrylamide gels, blotted on polyvinylidene difluoride (PVDF) membrane, and probed with appropriate antibodies as indicated elsewhere in the text. The following antibodies were used for immunoblotting: mouse monoclonal anti-FLAG (Sigma, 1:1,000), rabbit polyclonal anti-SM (1:500), rat polyclonal anti-DHX9 (EMD Millipore, 1:1,000), or rabbit polyclonal antitubulin (Sigma, 1:2,000). After extensive washing, blots were incubated in horseradish peroxidase-conjugated secondary goat anti-mouse (1:3,000), goat anti-rabbit (1:7,500), or goat anti-rat (1:2,000) antibodies (Sigma), and the membrane was washed, developed with a chemiluminescence reagent (Bio-Rad), and visualized on a Gel Documentation Station (Bio-Rad).

Knockdown of endogenous DHX9 with siRNA. Endogenous DHX9 in AGSiZ and HEK293-2089 cells was depleted by using SMARTpool with ON-TARGETplus DHX9 siRNA (Dharmacon; L-009950-00-0005 or J-009950-06-0002). siRNA transfections were performed with Lipofectamine RNAiMAX from ThermoFisher according to the manufacturer's protocol. Levels of endogenous DHX9 were measured by Western blotting using anti-DHX9 antibodies. The same membranes were stripped and probed with antitubulin to measure levels of tubulin as an internal loading control.

Quantification of infectious virion production. DHX9-depleted or mock-depleted AGSiZ cells were treated with doxycycline to induce viral lytic replication or mock induced. Cell supernatants were harvested at 5 days postinduction and filtered through 0.8-μm-pore cellulose acetate filters after centrifugation at 700 $\times$ *g* for 5 min. Filtered supernatants were used to infect 293T cells for 48 h at 37°C, 5% CO_2. The numbers of GFP-positive 293T cells representing infectious viral particles were quantitated by flow cytometry as previously described (11, 41). Three independent biological experiments were performed, and each sample was measured by flow cytometry in technical triplicates.

Quantification of viral DNA in cell pellets and supernatants. AGSiZ cells were depleted of DHX9 or mock depleted by siRNA transfections followed by treatment with doxycycline to induce viral lytic replication or mock induced. Cell pellets and supernatants were harvested at 3 days and 5 days postinduction, respectively. Total cellular and viral DNA was isolated from cell pellets by using the Qiagen Blood and Tissue DNeasy kit according to the manufacturer's protocol. The levels of intracellular viral DNAs were quantified with a primer pair specific for EBV BILF2 (forward, 5′-GGGAAGAAGACGACC AATAC-3′; reverse, 5′-TTGTGGTGTGGGAGACTAATG-3′) by qPCR. Amplification was performed with SYBR Green PCR Master Mix (Applied Biosystems), and GAPDH was used as the normalization control. For the analysis of DNA levels in cell supernatants, supernatants were harvested at 5 days and then filtered through 0.8-μm-pore cellulose acetate filters after centrifugation at 700 $\times$ *g* for 5 min. Filtered supernatant was centrifuged at 16,000 $\times$ *g* for 2 h at 4°C for virion concentration. After centrifugation, the supernatant was removed, the tube was inverted to dry on paper for 30 min, and the pellet was resuspended in 25 μl TBS by vortexing gently and incubated on ice for 30 min. A 2.5-μl amount of RQ1 DNase (1 U/μl stock) was added to each tube and incubated at 37°C for 30 min, 2.5 μl DNase Stop buffer was added, and the mixture was incubated at 65°C for 10 min. After DNase treatment, 0.3 μl proteinase K (10 mg/ml stock) was added and incubated at 55°C for 30 min. DNA samples were further purified by using the Qiagen Blood and Tissue DNeasy kit according to the manufacturer's protocol. Two microliters of isolated viral DNA was used to quantitate the relative viral copy number by qPCR with EBV BILF2 primers as described above. Three independent biological experiments were performed, and each sample was measured in technical triplicates.

Quantification of viral and cellular gene expression. Total RNA was isolated from treated AGSiZ and HEK293-2089 cells by using QIAzol and Qiagen miRNeasy mini kits according to the manufacturer's protocol. Viral transcripts were quantified by qRT-PCR with primer sets as we previously described (11, 41). Amplification was performed with Power SYBR Green RNA-to-C_T 1-Step kit (Applied Biosystems), and GAPDH was used as the endogenous control. Three independent biological experiments were performed, and each sample was measured in technical triplicates.

Immunofluorescence assays and microscopy. Cells grown on glass coverslips were transfected with different constructs using TransIT293 according to the manufacturer's protocol. At 48 h after transfection, cells were washed with 1× PBS, fixed and permeabilized with PBS containing 4% paraformaldehyde and 0.2% Triton X-100 for 15 to 20 min at room temperature, and then washed two times with 1× PBS followed by incubating with blocking buffer (20% goat serum in PBS) for 30 min at room temperature. Finally, the cells were incubated with appropriate primary antibodies in indicated dilution (anti-FLAG, 1:1,000 [Sigma]; anti-SM, 1:500; anti-DHX9, 1:200 [Santa Cruz sc-137232]) at 37°C for 1 h. The cells were washed three times with 1× PBS and incubated with secondary antibody goat anti-rat Alexa Fluor 594 IgG, goat anti-mouse Alexa Fluor 647, or goat anti-rabbit Alexa Fluor 647 IgG for 1 h at 37°C in the dark. Nuclear staining was performed with 4′,6-diamidino-2-phenylindole (DAPI) (Invitrogen). Images were collected and analyzed with a ZEISS Imager.M2 microscope system.

Luciferase reporter assays. For cells transfected with a cAMP response element (CRE)-luciferase reporter (pCRE-luc), each well of a 6-well plate was lysed with 100 μl of luciferase lysis reagent (Promega) at room temperature for 10 min. Cell debris was pelleted by brief centrifugation, and the supernatant was transferred to a new tube. Five microliters of cell lysate was mixed with 50 μl of luciferase assay reagent (Promega), and luminescence was measured with a Turner luminometer. The internal vector control (*Renilla*) reporter plasmid was cotransfected with the test reporter and used to normalize the reporter assay.

RNA sequencing and data analysis. cDNA libraries were prepared from total RNA by using the Illumina TruSeq Stranded Total RNA sample prep kit with Ribo-Zero Gold. Paired-end sequencing (2 × 150 bp) was performed on a NovaSeq system. Sequenced reads obtained from EBV-infected AGS cells were aligned to the human GRCh38 (GCF_000001405.38) genome. Reads were trimmed of adapters using Cutadapt 1.16 and then aligned to each reference database using STAR to output a BAM file sorted by coordinates. Mapped reads were assigned to annotated genes in the GTF files using featureCounts version 1.6.3 The output files from Cutadapt, FastQC, Picard CollectRNASeqMetrics, STAR, and featureCounts were summarized using MultiQC to check for any sample outliers. The counts from human genes were normalized, and differential gene expression was measured by using DESeq2 version1.20.0 (59). Functional annotation of genes is based on Gene Ontology (GO; http://www.geneontology.org). Enrichment analysis (overrepresentation) was performed to identify GO categories that might be enriched by the up- or downregulated genes.

ACKNOWLEDGMENTS

This work was supported by Public Health Service grant RO1 81133 (SS) from the National Cancer Institute and 1I01BX002262 (S.S.) from the VA ORD BLR&D.

RNA sequencing and bioinformatic analysis and flow cytometry were performed at the University of Utah Health Sciences and Huntsman Comprehensive Cancer Center Core Facilities. We thank Trenton Mel Church for his help in the luciferase experiments and Chris Stubben for bioinformatic analyses.

REFERENCES

1. Longnecker RM, Kieff E, Cohen JI. 2013. Epstein-Barr virus, p 1898–1959. *In* Knipe DM, Howley PM, Cohen JL, Griffin DE, Lamb RA, Martin MA, Racaniello VR, Roizman B (ed), Fields virology, 6th ed, vol 2. Lippincott Williams & Wilkins, Philadelphia, PA.
2. Hutt-Fletcher LM. 2016. The long and complicated relationship between Epstein-Barr virus and epithelial cells. J Virol 91:e01677-16. https://doi.org/10.1128/JVI.01677-16.
3. Li D, Fu W, Swaminathan S. 2018. Continuous DNA replication is required for late gene transcription and maintenance of replication compartments in gammaherpesviruses. PLoS Pathog 14:e1007070. https://doi.org/10.1371/journal.ppat.1007070.
4. Li H, Liu S, Hu J, Luo X, Li N, M Bode A, Cao Y. 2016. Epstein-Barr virus lytic reactivation regulation and its pathogenic role in carcinogenesis. Int J Biol Sci 12:1309–1318. https://doi.org/10.7150/ijbs.16564.
5. Gruffat H, Batisse J, Pich D, Neuhierl B, Manet E, Hammerschmidt W, Sergeant A. 2002. Epstein-Barr virus mRNA export factor EB2 is essential for production of infectious virus. J Virol 76:9635–9644.
6. Han Z, Marendy E, Wang YD, Yuan J, Sample JT, Swaminathan S. 2007. Multiple roles of Epstein-Barr virus SM protein in lytic replication. J Virol 81:4058–4069. https://doi.org/10.1128/JVI.02665-06.
7. Semmes OJ, Chen L, Sarisky RT, Gao Z, Zhong L, Hayward SD. 1998. Mta has properties of an RNA export protein and increases cytoplasmic accumulation of Epstein-Barr virus replication gene mRNA. J Virol 72:9526–9534.
8. Key SC, Yoshizaki T, Pagano JS. 1998. The Epstein-Barr virus (EBV) SM protein enhances pre-mRNA processing of the EBV DNA polymerase transcript. J Virol 72:8485–8492.
9. Verma D, Bais S, Gaillard M, Swaminathan S. 2010. Epstein-Barr virus SM protein utilizes cellular splicing factor SRp20 to mediate alternative splicing. J Virol 84:11781–11789. https://doi.org/10.1128/JVI.01359-10.
10. Ruvolo V, Gupta AK, Swaminathan S. 2001. Epstein-Barr virus SM protein interacts with mRNA in vivo and mediates a gene-specific increase in cytoplasmic mRNA. J Virol 75:6033–6041. https://doi.org/10.1128/JVI.75.13.6033-6041.2001.
11. Thompson J, Verma D, Li D, Mosbruger T, Swaminathan S. 2016. Identification and characterization of the physiological gene targets of the essential lytic replicative Epstein-Barr virus SM protein. J Virol 90:1206–1221. https://doi.org/10.1128/JVI.02393-15.
12. Nicewonger J, Suck G, Bloch D, Swaminathan S. 2004. Epstein-Barr virus (EBV) SM protein induces and recruits cellular Sp110b to stabilize mRNAs and enhance EBV lytic gene expression. J Virol 78:9412–9422. https://doi.org/10.1128/JVI.78.17.9412-9422.2004.
13. Hiriart E, Bardouillet L, Manet E, Gruffat H, Penin F, Montserret R, Farjot G, Sergeant A. 2003. A region of the Epstein-Barr virus (EBV) mRNA

export factor EB2 containing an arginine-rich motif mediates direct binding to RNA. J Biol Chem 278:37790–37798. https://doi.org/10.1074/jbc.M305925200.
14. Hiriart E, Farjot G, Gruffat H, Nguyen MV, Sergeant A, Manet E. 2003. A novel nuclear export signal and a REF interaction domain both promote mRNA export by the Epstein-Barr virus EB2 protein. J Biol Chem 278:335–342. https://doi.org/10.1074/jbc.M208656200.
15. Boyle SM, Ruvolo V, Gupta AK, Swaminathan S. 1999. Association with the cellular export receptor CRM 1 mediates function and intracellular localization of Epstein-Barr virus SM protein, a regulator of gene expression. J Virol 73:6872–6881.
16. Farjot G, Buisson M, Duc Dodon M, Gazzolo L, Sergeant A, Mikaelian I. 2000. Epstein-Barr virus EB2 protein exports unspliced RNA via a Crm-1-independent pathway. J Virol 74:6068–6076.
17. Ricci EP, Mure F, Gruffat H, Decimo D, Medina-Palazon C, Ohlmann T, Manet E. 2009. Translation of intronless RNAs is strongly stimulated by the Epstein-Barr virus mRNA export factor EB2. Nucleic Acids Res 37:4932–4943. https://doi.org/10.1093/nar/gkp497.
18. Lee T, Pelletier J. 2016. The biology of DHX9 and its potential as a therapeutic target. Oncotarget 7:42716–42739. https://doi.org/10.18632/oncotarget.8446.
19. Zhang S, Grosse F. 1997. Domain structure of human nuclear DNA helicase II (RNA helicase A). J Biol Chem 272:11487–11494.
20. Chakraborty P, Grosse F. 2010. WRN helicase unwinds Okazaki fragment-like hybrids in a reaction stimulated by the human DHX9 helicase. Nucleic Acids Res 38:4722–4730. https://doi.org/10.1093/nar/gkq240.
21. Fujii R, Okamoto M, Aratani S, Oishi T, Ohshima T, Taira K, Baba M, Fukamizu A, Nakajima T. 2001. A role of RNA helicase A in cis-acting transactivation response element-mediated transcriptional regulation of human immunodeficiency virus type 1. J Biol Chem 276:5445–5451. https://doi.org/10.1074/jbc.M006892200.
22. Kim T, Pazhoor S, Bao M, Zhang Z, Hanabuchi S, Facchinetti V, Bover L, Plumas J, Chaperot L, Qin J, Liu YJ. 2010. Aspartate-glutamate-alanine-histidine box motif (DEAH)/RNA helicase A helicases sense microbial DNA in human plasmacytoid dendritic cells. Proc Natl Acad Sci U S A 107:15181–15186. https://doi.org/10.1073/pnas.1006539107.
23. Reddy TR, Tang H, Xu W, Wong-Staal F. 2000. Sam68, RNA helicase A and Tap cooperate in the post-transcriptional regulation of human immunodeficiency virus and type D retroviral mRNA. Oncogene 19:3570–3575. https://doi.org/10.1038/sj.onc.1203676.
24. Sadler AJ, Latchoumanin O, Hawkes D, Mak J, Williams BR. 2009. An antiviral response directed by PKR phosphorylation of the RNA helicase A. PLoS Pathog 5:e1000311. https://doi.org/10.1371/journal.ppat.1000311.
25. Sheng C, Yao Y, Chen B, Wang Y, Chen J, Xiao M. 2013. RNA helicase is involved in the expression and replication of classical swine fever virus and interacts with untranslated region. Virus Res 171:257–261. https://doi.org/10.1016/j.virusres.2012.11.014.
26. Westberg C, Yang JP, Tang H, Reddy TR, Wong-Staal F. 2000. A novel shuttle protein binds to RNA helicase A and activates the retroviral constitutive transport element. J Biol Chem 275:21396–21401. https://doi.org/10.1074/jbc.M909887199.
27. Wodrich H, Schambach A, Krausslich HG. 2000. Multiple copies of the Mason-Pfizer monkey virus constitutive RNA transport element lead to enhanced HIV-1 Gag expression in a context-dependent manner. Nucleic Acids Res 28:901–910. https://doi.org/10.1093/nar/28.4.901.
28. Xing L, Niu M, Kleiman L. 2012. In vitro and in vivo analysis of the interaction between RNA helicase A and HIV-1 RNA. J Virol 86:13272–13280. https://doi.org/10.1128/JVI.01993-12.
29. Yang JP, Tang H, Reddy TR, Wong-Staal F. 2001. Mapping the functional domains of HAP95, a protein that binds RNA helicase A and activates the constitutive transport element of type D retroviruses. J Biol Chem 276:30694–30700. https://doi.org/10.1074/jbc.M102809200.
30. Zhang Z, Yuan B, Lu N, Facchinetti V, Liu YJ. 2011. DHX9 pairs with IPS-1 to sense double-stranded RNA in myeloid dendritic cells. J Immunol 187:4501–4508. https://doi.org/10.4049/jimmunol.1101307.
31. Tang H, Gaietta GM, Fischer WH, Ellisman MH, Wong-Staal F. 1997. A cellular cofactor for the constitutive transport element of type D retrovirus. Science 276:1412–1415.
32. Tang H, Wong-Staal F. 2000. Specific interaction between RNA helicase A and Tap, two cellular proteins that bind to the constitutive transport element of type D retrovirus. J Biol Chem 275:32694–32700. https://doi.org/10.1074/jbc.M003933200.
33. Li J, Tang H, Mullen TM, Westberg C, Reddy TR, Rose DW, Wong-Staal F. 1999. A role for RNA helicase A in post-transcriptional regulation of HIV type 1. Proc Natl Acad Sci U S A 96:709–714.
34. Ranji A, Shkriabai N, Kvaratskhelia M, Musier-Forsyth K, Boris-Lawrie K. 2011. Features of double-stranded RNA-binding domains of RNA helicase A are necessary for selective recognition and translation of complex mRNAs. J Biol Chem 286:5328–5337. https://doi.org/10.1074/jbc.M110.176339.
35. Lenarcic EM, Ziehr BJ, Moorman NJ. 2015. An unbiased proteomics approach to identify human cytomegalovirus RNA-associated proteins. Virology 481:13–23. https://doi.org/10.1016/j.virol.2015.02.008.
36. Liao HJ, Kobayashi R, Mathews MB. 1998. Activities of adenovirus virus-associated RNAs: purification and characterization of RNA binding proteins. Proc Natl Acad Sci U S A 95:8514–8519.
37. Paingankar MS, Arankalle VA. 2015. Identification and characterization of cellular proteins interacting with hepatitis E virus untranslated regions. Virus Res 208:98–109. https://doi.org/10.1016/j.virusres.2015.06.006.
38. Lin L, Li Y, Pyo HM, Lu X, Raman SN, Liu Q, Brown EG, Zhou Y. 2012. Identification of RNA helicase A as a cellular factor that interacts with influenza A virus NS1 protein and its role in the virus life cycle. J Virol 86:1942–1954. https://doi.org/10.1128/JVI.06362-11.
39. Rahman MM, Bagdassarian E, Ali MAM, McFadden G. 2017. Identification of host DEAD-box RNA helicases that regulate cellular tropism of oncolytic Myxoma virus in human cancer cells. Sci Rep 7:15710. https://doi.org/10.1038/s41598-017-15941-1.
40. Ahmad S, Hur S. 2015. Helicases in antiviral immunity: dual properties as sensors and effectors. Trends Biochem Sci 40:576–585. https://doi.org/10.1016/j.tibs.2015.08.001.
41. Verma D, Thompson J, Swaminathan S. 2016. Spironolactone blocks Epstein-Barr virus production by inhibiting EBV SM protein function. Proc Natl Acad Sci U S A 113:3609–3614. https://doi.org/10.1073/pnas.1523686113.
42. Aubry V, Mure F, Mariame B, Deschamps T, Wyrwicz LS, Manet E, Gruffat H. 2014. Epstein-Barr virus late gene transcription depends on the assembly of a virus-specific preinitiation complex. J Virol 88:12825–12838. https://doi.org/10.1128/JVI.02139-14.
43. Gruffat H, Marchione R, Manet E. 2016. Herpesvirus late gene expression: a viral-specific pre-initiation complex is key. Front Microbiol 7:869. https://doi.org/10.3389/fmicb.2016.00869.
44. El-Guindy A, Lopez-Giraldez F, Delecluse HJ, McKenzie J, Miller G. 2014. A locus encompassing the Epstein-Barr virus bglf4 kinase regulates expression of genes encoding viral structural proteins. PLoS Pathog 10:e1004307. https://doi.org/10.1371/journal.ppat.1004307.
45. Gruffat H, Kadjouf F, Mariame B, Manet E. 2012. The Epstein-Barr virus BcRF1 gene product is a TBP-like protein with an essential role in late gene expression. J Virol 86:6023–6032. https://doi.org/10.1128/JVI.00159-12.
46. Tetsuka T, Uranishi H, Sanda T, Asamitsu K, Yang JP, Wong-Staal F, Okamoto T. 2004. RNA helicase A interacts with nuclear factor kappaB p65 and functions as a transcriptional coactivator. Eur J Biochem 271:3741–3751. https://doi.org/10.1111/j.1432-1033.2004.04314.x.
47. Garcia-Sastre A, Biron CA. 2006. Type 1 interferons and the virus-host relationship: a lesson in detente. Science 312:879–882. https://doi.org/10.1126/science.1125676.
48. Mittnacht S, Straub P, Kirchner H, Jacobsen H. 1988. Interferon treatment inhibits onset of herpes simplex virus immediate-early transcription. Virology 164:201–210.
49. Dupuis S, Jouanguy E, Al-Hajjar S, Fieschi C, Al-Mohsen IZ, Al-Jumaah S, Yang K, Chapgier A, Eidenschenk C, Eid P, Al Ghonaium A, Tufenkeji H, Frayha H, Al-Gazlan S, Al-Rayes H, Schreiber RD, Gresser I, Casanova JL. 2003. Impaired response to interferon-alpha/beta and lethal viral disease in human STAT1 deficiency. Nat Genet 33:388–391. https://doi.org/10.1038/ng1097.
50. Nakajima T, Uchida C, Anderson SF, Lee CG, Hurwitz J, Parvin JD, Montminy M. 1997. RNA helicase A mediates association of CBP with RNA polymerase II. Cell 90:1107–1112.
51. Aratani S, Fujii R, Oishi T, Fujita H, Amano T, Ohshima T, Hagiwara M, Fukamizu A, Nakajima T. 2001. Dual roles of RNA helicase A in CREB-dependent transcription. Mol Cell Biol 21:4460–4469. https://doi.org/10.1128/MCB.21.14.4460-4469.2001.
52. Capitanio JS, Montpetit B, Wozniak RW. 2017. Human Nup98 regulates the localization and activity of DExH/D-box helicase DHX9. Elife 6:e18825. https://doi.org/10.7554/eLife.18825.
53. Capitanio JS, Montpetit B, Wozniak RW. 2018. Nucleoplasmic Nup98

controls gene expression by regulating a DExH/D-box protein. Nucleus 9:1–8. https://doi.org/10.1080/19491034.2017.1364826.
54. Lee T, Di Paola D, Malina A, Mills JR, Kreps A, Grosse F, Tang H, Zannis-Hadjopoulos M, Larsson O, Pelletier J. 2014. Suppression of the DHX9 helicase induces premature senescence in human diploid fibroblasts in a p53-dependent manner. J Biol Chem 289:22798–22814. https://doi.org/10.1074/jbc.M114.568535.
55. Hartman TR, Qian S, Bolinger C, Fernandez S, Schoenberg DR, Boris-Lawrie K. 2006. RNA helicase A is necessary for translation of selected messenger RNAs. Nat Struct Mol Biol 13:509–516. https://doi.org/10.1038/nsmb1092.
56. Fuchsova B, Novak P, Kafkova J, Hozak P. 2002. Nuclear DNA helicase II is recruited to IFN-alpha-activated transcription sites at PML nuclear bodies. J Cell Biol 158:463–473.
57. Anderson SF, Schlegel BP, Nakajima T, Wolpin ES, Parvin JD. 1998. BRCA1 protein is linked to the RNA polymerase II holoenzyme complex via RNA helicase A. Nat Genet 19:254–256. https://doi.org/10.1038/930.
58. Delecluse HJ, Hilsendegen T, Pich D, Zeidler R, Hammerschmidt W. 1998. Propagation and recovery of intact, infectious Epstein-Barr virus from prokaryotic to human cells. Proc Natl Acad Sci U S A 95:8245–8250.
59. Love MI, Huber W, Anders S. 2014. Moderated estimation of fold change and dispersion for RNA-seq data with DESeq2. Genome Biol 15:550. https://doi.org/10.1186/s13059-014-0550-8.